Soft Matter

Accepted Manuscript

ROYAL SOCIETY OF CHEMISTRY

www.rsc.org/softmatter

Stick-Slip Water Penetration into Capillaries Coated with Swelling Hydrogel

J.E. Silva[a], R. Geryak[b], D.A. Loney[c] , P.A. Kottke[a], R.R. Naik[c], V.V. Tsukruk[b], A.G. Fedorov*[a,d]

[a] *Department of Mechanical Engineering, Georgia Institute of Technology, Atlanta, GA 30332, USA*
[b] *Department of Materials Science and Engineering, Georgia Institute of Technology, Atlanta, GA 30332, USA*
[c] *Materials and Manufacturing Directorate, Air Force Research Laboratory, Wright-Patterson Air Force Base, OH 45433, USA*
[d] *Parker H. Petit Institute for Bioengineering and Biosciences and Renewable Bioproducts Institute, Georgia Institute of Technology, Atlanta, GA 30332, USA. Email: AGF@gatech.edu*

Abstract

We have observed intriguing stick-slip behavior during capillary pressure driven filling of borosilicate microtubes coated with hydrogel on their inner wall. Swelling of hydrogel upon exposure to a translating waterfront is accompanied by "stick-and-slip" motion. This results in the macroscopic filling velocity for water penetration into glass capillaries coated with poly(*N*-isopropylacrylamide) (PNIPAM) being constant throughout the filling process, and reduced by three orders of magnitude when compared to filling of uncoated capillaries. A simple scaling analysis is used to introduce a possible explanation by considering the mechanisms responsible for pinning and unpinning of the contact line. The explanation assumes that the time scale for water diffusion into a hydrogel film and the resulting swelling/change of the local meniscus contact angle define the duration of each "stick" event. The "slip" length scale is in turn established by the elastocapillary deformation of dry hydrogel at the pinning point of the contact line. The sequential dynamics of these processes then determine the rate of water filling into a swelling capillary. Collectively, these experimental and theoretical results provide a new conceptual framework for liquid motion confined by soft, dynamically evolving polymer interfaces, in which the system creates an energy barrier to further motion through elasto-capillary deformation, and then lowers the barrier through diffusive softening. This insight has implications for optimal design of microfluidic and lab-on-a-chip devices based on stimuli-responsive smart polymers.

I. Introduction

Responsive soft materials can be designed from a wide variety of components, which in many cases include stimuli responsive hydrogels.[1] Weakly-crosslinked hydrogels are capable of significant swelling-deswelling behavior by imbibing and releasing water anywhere from 2 to 500 times their weight, [2, 3] and these materials have become ubiquitous across a wide range of research applications, including drug delivery,[4-6] microfluidics,[7-9] and agriculture.[10] Further interest has stemmed from the synthesis of stimuli-responsive or smart polymers, which undergo conformational changes in response to stimuli including temperature, pH, and electromagnetic fields. [11,12,13,14, 15]

Hydrogel surface properties have important implications for interface manipulation. Hydrogel wettability changes due to swelling and can be modulated by external stimuli in the case of smart polymer hydrogels.[16, 17] While wetting on hard surfaces such as metals is understood through models and theory proposed by Young-Dupré,[18] Wenzel,[19] and Cassie-Baxter [20], in the case of soft materials such as hydrogels, local deformations near the contact line make the problem more complex. Changes of hydrogel substrate shape can come as a result of local swelling upon liquid uptake, as well as elastocapillary deformation induced by the vertical component of the surface tension force acting along the free surface at the contact line of liquid-impermeable soft materials.

Earlier research efforts have examined contact line evolution for droplets deposited on non-swelling gels,[21, 22] in which there is no mass exchange between the substrate and the droplets. In such instances, where surface deformations occur strictly due to the vertical component of the surface tension force, substrate deformation has a significant effect on contact line dynamics of the fluid motion. For example, Kajiya *et al*. demonstrated stick-slip contact line

motion for droplets growing on SBS-paraffin gels.[23] When the characteristic droplet inflation rate is on the order of the gel surface deformation rate, local ridges form due to elastocapillary deformation to pin the contact line before allowing it to slip forward and repeat the process. Similar stick-slip motion has been reported for a variety of liquids (formamide, glyceorl, ethylene glycol, and paraffin oil) on viscoelastic acrylic polymer films.[24, 25]

Recently, Kajiya *et al*.[26] examined contact line dynamics for a droplet placed on the surface of an initially dry, swelling hydrogel and observed interrelated dynamics of the resulting hydrogel swelling and droplet shrinking due to water uptake by the substrate. Initially, the contact line remains pinned despite the decreasing apparent contact angle associated with decreasing droplet volume as liquid from the droplet diffuses into the hydrogel. Contact line depinning and subsequent droplet uptake by the substrate occurs upon exceeding a critical lateral extent of the swollen hydrogel surface. Through a series of scaling arguments largely based on the local geometry, Kajiya *et al.* were able to model gel deformation and droplet contact angle evolution to predict the time to unpin the contact line.

The current work examines contact line stick-slip motion resulting from a swelling hydrogel coating inside a capillary during capillary filling, thus introducing a novel geometry and incorporating the effect of polymer confinement on the dynamics of the fluid flow. PNIPAM is chosen based on previous experience in synthesizing the hydrogel, with temperature-responsive properties unexplored in this particular application. We first demonstrate constant filling velocity of water in PNIPAM coated capillaries, and contrast this behavior to filling behavior of water in uncoated capillaries, as well as the filling behavior of glycerol in coated and uncoated capillaries. With the exception of the case of water in hydrogel coated capillaries, all of these systems demonstrate behaviors in line with previous studies of capillary filling.[27] Furthermore,

observation of the meniscus during filling indicates the presence of stick-slip motion for water in a PNIPAM coated capillary but not for the other filling experiments, suggesting that hydrogel swelling is also necessary for stick-slip motion. Macroscopically, this results in an unexpectedly constant meniscus propagation velocity during water filling of capillaries in the presence of hydrogel. Based on this observation, we develop a simple scaling framework that ties stick-slip behavior in the hydrogel capillary system to repeated sequences of contact line pinning and unpinning. Importantly, this framework explains the apparently constant macroscopic velocity of the meniscus motion during the entire period of capillary filling. While this stick-and-slip process has been demonstrated in other applications, this study is the first to investigate repeated stick-slip events governed by elastocapillary interactions and mass transfer in thin hydrogel films for a confined geometry relevant to microfluidic applications. Collectively, these experimental and theoretical results provide important insight into liquid motion confined by soft, dynamically evolving polymer interfaces, with implications to optimal design of lab-on-a-chip devices based on stimuli-responsive smart polymers. The practical impact of this work is also significant as it demonstrates new hydrogel synthesis methods, which are easy to implement in basic laboratory environments without use of specialized equipment, and carry broad applicability to confined microfluidic topologies of different geometries.

II. Experimental Methods

a) Synthesis of PNIPAM Hydrogel Films Coating the Inner Walls of Glass Capillaries

Borosilicate glass capillaries from Sutter Instruments of two different inner diameters (300μm and 750μm) were purchased from VWR. N,N'-methylenebisacrylamide (MBA 99%, polymer cross-linking agent), ammonium persulfate (APS 99.99+%, initiator), and tetramethylethylenediamine (TEMED 99%, catalyst) were all purchased from Aldrich, while NIPAM (97%) was purchased from Tokyo Chemical

Industry. Prior to synthesizing the PNIPAM hydrogel layer, the capillaries were cleaned using piranha solution. Capillaries were then silanized in order to form a bonding layer on the glass for the PNIPAM hydrogel[28] by immersing them in a 0.6 wt% solution of vinyltrimethoxysilane (VTMS 97%, Aldrich) in toluenefor 2 hours at room temperature. After silanization, the capillaries were rinsed in Nanopure water and dried with flowing air.

NIPAM precursor solution was prepared by adding 0.4745g NIPAM, 0.0830g MBA, and 25μL of TEMED to 10mL of Nanopure water (18.2 MΩ-cm resistivity). The solution was vigorously mixed for 5 minutes, and stored at 5°C. When synthesizing the PNIPAM hydrogel coatings, 1mL of precursor solution was mixed with 1.00mg APS in order to initiate the gelling process. Using a pipette, a droplet of this mixture was introduced to one end of a silanized capillary and allowed to fill the inner volume through capillary action. The capillary was then placed vertically (to allow for uniform surface contact between the capillary inner diameter and curing precursor gel solution) into a furnace set at 75°C and allowed to cure for 12 hours. Upon removal, an examination of the capillary ends shows a build-up of polymer residue left behind during the curing process. However, removal of the capillary ends reveals a coating of roughly uniform thickness along the majority of the capillary length.

By controlling the amount of NIPAM in the stock solution, it is possible to control the thickness of the resultant polymer layer. For polymer layers synthesized in 750μm ID capillaries with equivalent amounts of MBA and TEMED, precursor solution with 1.93g NIPAM gives a dry coating thickness of 42+/-8μm, while solution with 0.59g NIPAM

gives 13+/-2 μm (Fig. 1a). Film thickness measurements were taken for multiple samples, and error is reported with a 95% confidence interval.

Table 1 provides data for samples used in all experiments, synthesized following the above procedure with 0.4745g NIPAM. Data shows the dry and swollen thicknesses for the hydrogel layers, with error bars based on multiple measurements of dry/swollen thickness. Dry PNIPAM coatings synthesized per this procedure that are less than 20μm thick take roughly 1-2 seconds to reach equilibrium thickness upon hydration (Fig. 1b).

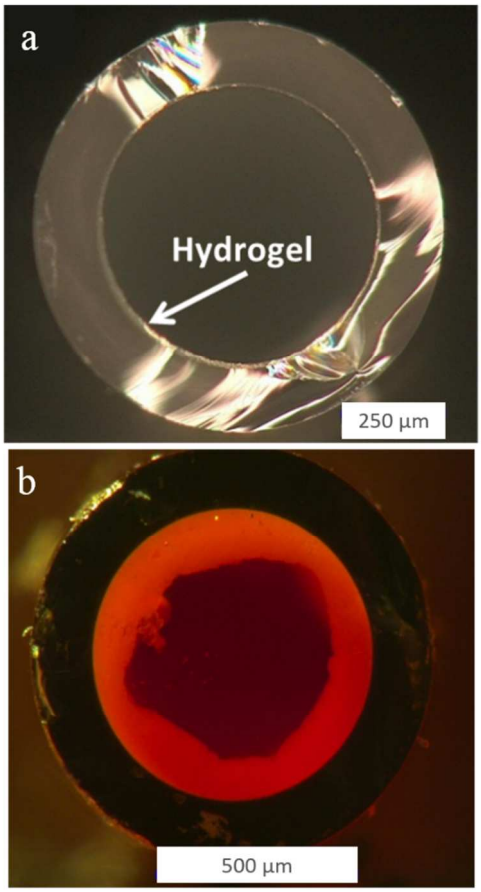

Figure 1: 750μm ID capillary with 13±2μm coating of unswollen PNIPAM hydrogel (a) shown in (b) after swelling due to hydration. The swollen hydrogel (b) is red due to added food coloring for contrast.

Table 1: Hydrogel thickness measurements for capillaries coated with PNIPAM hydrogel on inner walls

Sample Number	Capillary ID	Gel Dry Thickness	Gel Swollen

	(μm)	(μm)	Thickness (μm)
1	300	8 ± 0.5	19 ± 1
2	300	8 ± 0.7	23 ± 1
3	750	12 ± 2	63 ± 7
4	750	12 ± 2	53 ± 7

b) Visualization

In order to simultaneously record the liquid meniscus motion and hydrogel swelling behavior, a two camera system was employed (Fig. 2). The sample to be studied was placed on a segment of two-sided tape and positioned beneath a Keyence Digital Microscope VHX-500F imaging at 30fps. Additionally, a MEGAPLUS Redlake ES 1.0 camera (also imaging at 30fps) was used to capture back-end view of the sample, i.e., to record hydrogel swelling in real time.

At the start of each experiment, a droplet of liquid (approximately 10 times the capillary volume) was introduced at the front end of the capillary (opposite end from which the Redlake camera records data), and allowed to wick through via capillary action. As the meniscus travelled through the sample, the Keyence microscope recorded its

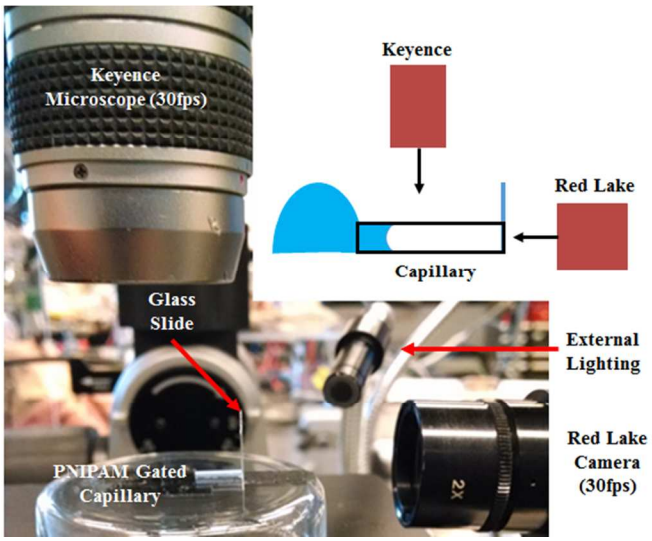

progress (see, for example, Supporting Information Video 1). Once the meniscus reached the end of the capillary, the Redlake camera captured swelling data (see Supporting Information Video 2). A glass slide was placed at this end of the capillary so as to prevent distortion from a curved liquid interface.

Figure 2: Experimental setup for simultaneous capture of meniscus position and hydrogel swelling kinetics during capillary filling.

III. Experimental Results and Discussion

Macroscopically Constant Velocity Observed Only for Water Filling a PNIPAM Coated Capillary

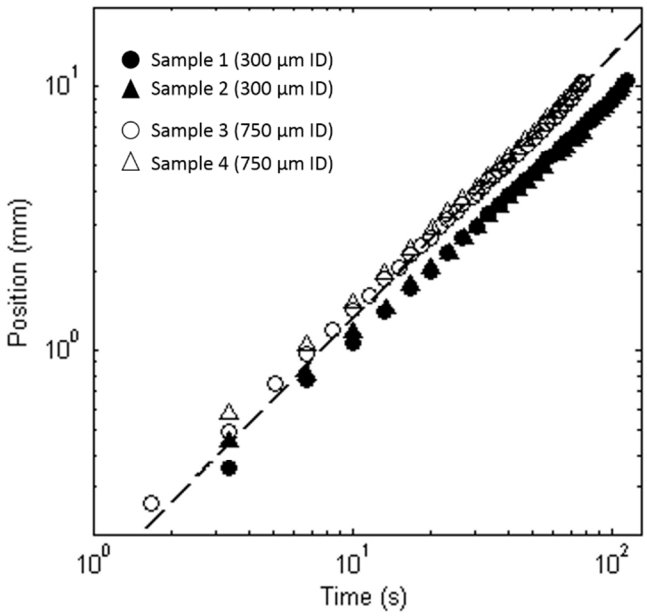

Figure 2: Meniscus position vs. time extracted from images such as those in Supporting Information Video 1. Data for Samples 1 and 2 are from 300µm ID PNIPAM gated samples, while data from Samples 3 and 4 are from 750µm ID PNIPAM gated capillaries. The dashed line is a reference line of slope unity. Dry and swollen PNIPAM layer thicknesses are provided in Table I.

Figure 3 shows the meniscus position for water propagating through capillaries coated with PNIPAM hydrogel, with the sample numbers indicated in the legend corresponding to the data in Table 1. In all cases, measurements show consistently linear behavior, e.g., capillary filling at a constant velocity through the entire process. The apparent velocities extracted from

these data are $145 \pm 9\,^{\mu m}/_{s}$ for 750μm ID capillaries and $99 \pm 5\,^{\mu m}/_{s}$ for the 300μm ID capillaries.

The results in Figure 3, in which meniscus position, $x_m(t)$, is linearly proportional to the filling time, are distinctly different from typical behavior for both water and glycerol in capillaries without a PNIPAM coating (see Figs. 4 and 5). In particular, Fig. 5 highlights that glycerol, which does not induce swelling of PNIPAM hydrogels, does not exhibit a constant meniscus velocity when filling a capillary coated with PNIPAM. Previous hydrodynamic investigations of capillary filling have shown the existence of three regimes of filling behavior: (i) inertial filling, in which capillary forces accelerate the liquid and meniscus position increases with the square of time, i.e., $x_m \sim t^2$; (ii) convective filling, in which the flow profile develops and the meniscus position increases linearly with time, i.e., $x_m \sim t$; and, (iii) the viscous, or Washburn, regime, in which the flow is fully developed and capillary forces are balanced by wall shear stresses, leading to meniscus position increasing with the square root of time, i.e., $x_m \sim \sqrt{t}$.[27] Plots of meniscus position as a function time for water filling bare capillaries and for glycerol filling coated and uncoated capillaries are presented in Figs. 4 and 5, respectively. These plots are on a logarithmic scale and in all cases a transition occurs from behavior consistent with inertial filling (thin solid line) to convective filling (dashed line), and then to the Washburn regime (solid line).

In contrast, the plot of meniscus position as a function of time for water filling PNIPAM coated capillaries, Fig. 3, shows no transitions, thus suggesting that a different physics must be in play for defining water transport in these capillaries. In fact, the duration of the constant velocity filling, ~ 100 s, is much longer than that predicted using the time scales reported by Stange et al., $\rho R^2/(8\mu) \sim 0.01$ s,[27] as observed in Fig. 4. Significantly, the presence of PNIPAM reduced the

water filling rate by several orders of magnitude, while it did not have the same impact on the glycerol filling rate.

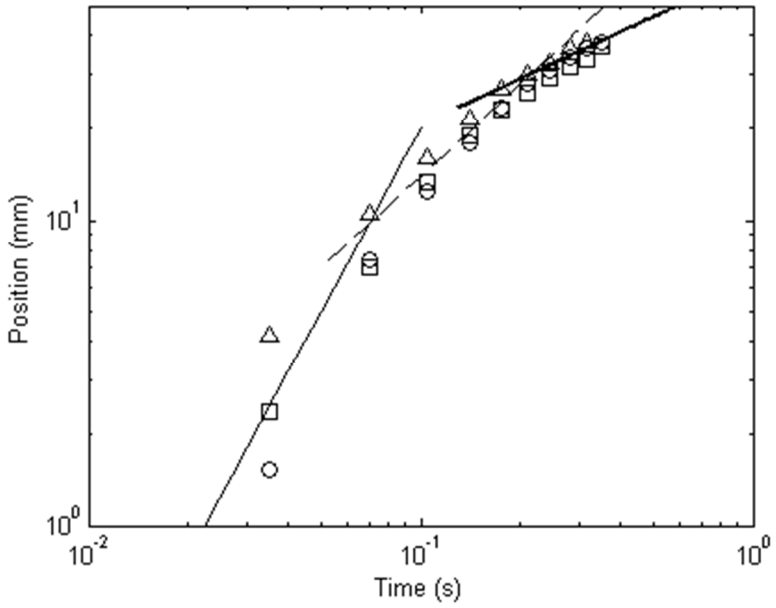

Figure 4: Meniscus position vs. time for water in bare, uncoated glass capillaries, 750µm ID. The three different symbols are data from three separate experiments using the same capillary. The thin line is a line of slope 2 (corresponding to inertial filling behavior), the dashed line is of slope 1 (corresponding to the convective loss regime), and the thick line is slope ½ (corresponding to the Washburn regime).

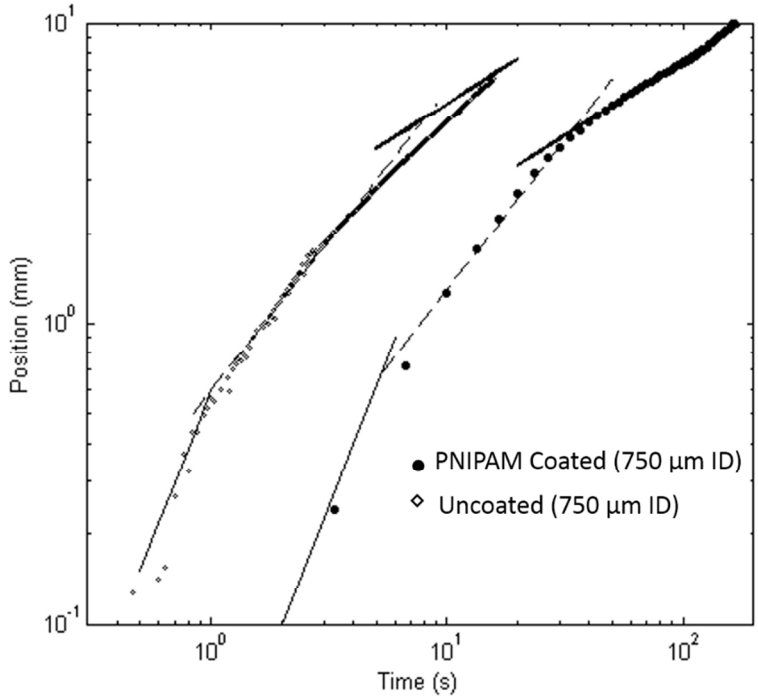

Figure 5: Meniscus position vs. time for glycerol in a bare, uncoated glass capillary with 750µm ID (open diamonds) and PNIPAM coated glass capillary with 750µm ID (filled circles). The thin lines are lines of slope 2

(corresponding to inertial filling behavior), the dashed lines have slope 1 (corresponding to the convective loss regime), and the thick lines have slope ½ (corresponding to the Washburn regime). The shift to longer times is due to higher contact angle for glycerol on PNIPAM than on glass.

Filling of PNIPAM Coated Capillaries is Governed by Contact Line Stick-and-Slip Sequence

The microscopic origin of the slower than expected filling behavior is revealed by meniscus tracking experiments, using the same procedure as shown in Figure 2, but repeated under higher magnification (200X). Local contact line motion was tracked over 700μm sections of PNIPAM gated capillaries (300 μm ID) with images captured at 0.03 s intervals. Video of the meniscus motion is provided in Supporting Information Video 3. As is apparent in Video 3 (top), the water meniscus motion has a stop-and-go nature, which can be described as a series of stick events (when the contact line is momentarily stabilized in position), followed by slip events (in which the meniscus advances before pinning again). The quantitative determination of the stick delay time and the slip distance is difficult due to both low frame rate of the available cameras, and difficulty in precisely defining the meniscus interface position inside the PNIPAM coated capillaries. Video 3 (bottom) shows the smoother propagation of glycerol through a PNIPAM coated capillary. The meniscus positions from Video 3, determined using MATLAB's image processing capabilities, are plotted in Figure 6. Comparison of the smooth increase of the glycerol meniscus position as compared to the water meniscus position, which shows numerous jumps and stalls, is consistent with the hypothesis that stick-slip motion is responsible for the anomalous motion of water into PNIPAM coated capillaries.

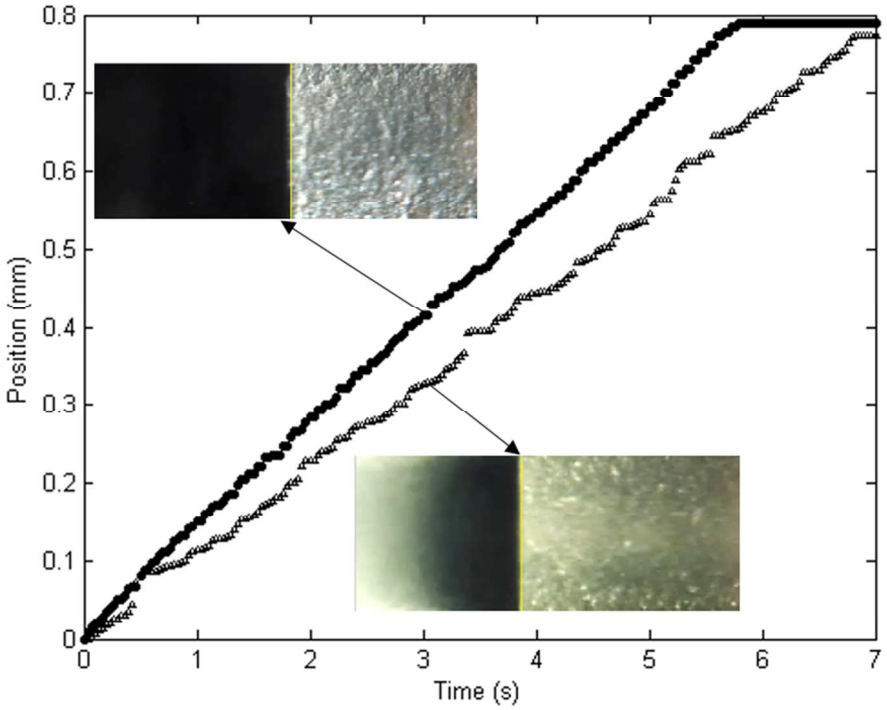

Figure 6: Meniscus position vs. time for water (open triangles) and glycerol (filled circles) in PNIPAM coated glass capillaries with 300μm ID glass capillaries. The inset above the curves show the detected meniscus position for glycerol at 3 s, and the inset below shows the detected meniscus position for water at 3 s (in both insets, the liquid is penetrating from left to right, and the detected meniscus position is indicated with a thin line).

IV. Scaling Analysis of Stick-Slip Behavior

Based on the stop-and-go motion observed in the high magnification video of water motion in PNIPAM coated capillaries, e.g., Supporting Information Video 3 (top), we have postulated that the motion of the contact line through the PNIPAM coated capillary is a repeated series of stick-and-slip events. Depicted schematically in Figures 7 and 8, this description is consistent with similar physics observed in water droplet behavior on top of a planar swelling hydrogel surface.[26] At the end of a slip phase (Fig. 8 a), the advancing contact line pins due to surface interactions upon encountering dry hydrogel, where literature reported values of advancing contact angles near 90º.[29] Contact line pinning begins the stick phase (Fig. 8 b-c), and once the contact line motion halts, capillary pressure induced flow rapidly flattens the meniscus. The local contact angle is modified by elastocapillary deformation of polymer (Fig. 8 c-d).

Several studies reporting soft surface profiles due to elastocapillary deformation in the vicinity of contact lines [30, 31] indicate lateral extent of deformation is of the order of the elastocapillary length scale, L_{ec}. For water and dry PNIPAM hydrogel, $L_{ec} = \gamma/E = 0.7\mu$m, given the surface tension of water $\left(\gamma = 0.072\,{}^{\mathrm{N}}/_{\mathrm{m}}\right)$ and Young's modulus for dry PNIPAM ($E \sim 10^5$Pa).[32] As water diffuses into the hydrogel, swelling occurs and the position of the partially hydrated region begins to extend downstream of the pinned contact line, changing both the bulk properties of the gel (such as the Young's modulus) and the surface properties (Fig. 8 d). The Young's modulus of completely hydrated PNIPAM is at least an order of magnitude smaller than that of dry hydrogel, indicating that as the hydrogel swells, elastocapillary deformation will become more significant.[32-34] Furthermore, the advancing contact angle of water on swollen PNIPAM, 45º,[29] is much smaller than that on the dry hydrogel. The combined effects of swelling, reduction in advancing contact angle, and increased elastic deformation result in unpinning, and the contact line moves forward with the hydrated PNIPAM advancing contact angle (Fig. 8 a) until it reaches the end of the water diffusion front and the beginning of the completely dry PNIPAM, where it pins again.

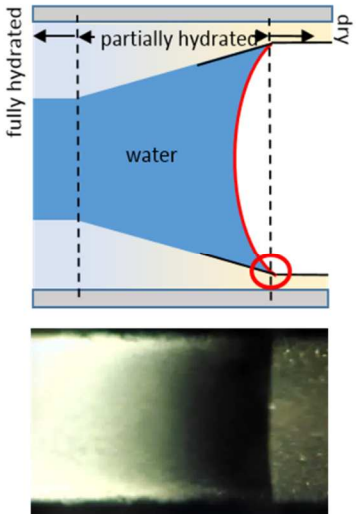

Figure 7: Conceptual framework for understanding the stick-slip behavior observed in filling of PNIPAM coated capillaries with water (top). The region circled in red is the contact line region, which is the focus of Fig. 8, and the

meniscus shape in both figures is given by a red curve. The image in the bottom is of the same region in a capillary during water filling; as in the top figure, the meniscus motion is from left to right.

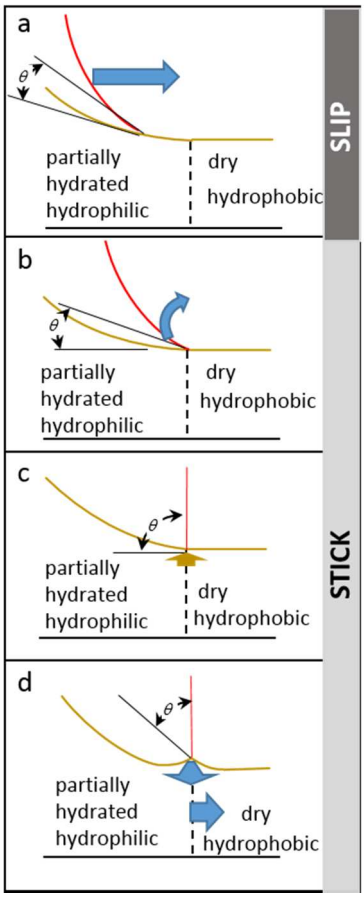

Figure 8: Depiction of events occurring in the contact line region highlighted in Fig. 7 (top) that lead to pinning and unpinning, and thus stick-and-slip behavior. (a) During slip, the contact angle is small due to hydrophilic, partially wetted PNIPAM, resulting in an advancing negative curvature interface. (b) When the contact line reaches the dry PNIPAM, it stops and the interface adjusts to become nearly flat. (c) The polymer film deforms at the contact line, pulled vertically by surface tension. (d) As water diffuses into the PNIPAM, it softens the polymer and changes its wetting properties.

The capillary-driven slip flow events occur on the time scale, t_{slip}, required for meniscus motion through a single slip displacement, L_{slip}. For short displacements, i.e., less than one capillary radius, capillary forces are balanced by inertial forces, and the slip time scale is $t_{slip} \sim \sqrt{\rho R^2 L_{slip}/\gamma}$.[27] Slip time will have a negligible impact on the apparent velocity if it is much smaller than the time over which "stick" occurs. Hence, in this case, the apparent meniscus

velocity can be expressed to leading order in terms of the slip displacement along the capillary, and the time over which stick occurs, i.e., $v_{\mathrm{app}} = L_{\mathrm{slip}}/t_{\mathrm{stick}}$.

From the hypothesized description of stick-slip behavior depicted in Fig. 8, L_{slip} is the diffusional length scale, $L_{\mathrm{slip}} \sim \sqrt{D t_{\mathrm{stick}}}$. Thus, given an experimentally obtained apparent velocity and diffusion coefficient, we can find the associated slip displacement and stick times under the assumption that slip times are much faster than stick times. Taking $D = 1 \times 10^{-10}\ \mathrm{m^2/s}$ [35] and equating v_{app} to the macroscopic, apparent velocity values observed experimentally, we find that $t_{\mathrm{stick}} = 4.8 \pm 6\ \mathrm{ms}$ and $L_{\mathrm{slip}} = 0.69 \pm 0.04\ \mu\mathrm{m}$ for 750μm ID capillaries, and $t_{\mathrm{stick}} = 10.7 \pm 1.5\ \mathrm{ms}$ and $L_{\mathrm{slip}} = 1.03 \pm 0.7 \mu\mathrm{m}$ for 300μm ID capillaries. These estimates are consistent with apparent velocity predictions based on unpinning criteria in which the diffusional length scale and the elastocapillary length are equated, although other sources of contact line pinning, besides elastocapillary deformation, cannot be ruled out. Furthermore, these stick times are both much longer than the slip times associated with the slip lengths. The observed capillary filling times do, however, show a slight dependence on capillary radius, with the smaller radius capillaries filling somewhat more slowly. This trend is not captured by the proposed scaling, in which, to leading order, the filling speed is determined by a balance of elastocapillary length with the local diffusion length, neither of which depend on the capillary radius. The most likely explanation of this trend is through the impact of overall capillary radius on the slip time, which is treated as instantaneous in our analysis. In fact, the slip velocity increases monotonically with capillary radius, and thus the accumulated effect of the different slip times between the two capillary sizes could explain the different apparent velocities.

The above scaling analysis and the experimental observations both indicate that water capillary pressure driven penetration into a hydrogel-lined microtube is dominated by stick–slip behavior. We have proposed a model in which sticking occurs due to elastocapillary pinning, with diffusion of water into the deformed, dry hydrogel resulting in relaxation of the substrate and subsequent slip. This finding is in contrast to the similar works of Kajiya et al., [26] who found that lateral deformation of hydrogel beyond the water contact line was elastic in nature. Given the relatively large scale of the problem studied in the work of Kajiya et al. (on the order of millimeters), these elastic effects dominated diffusive ones over the timescales of interest. Applying the basis of Kajiya's analysis here, the appropriate scaling would be to take the slip displacement, $\boldsymbol{L_{slip}}$, as the capillary radius, which would result in apparent velocities orders of magnitude smaller than those observed. Although the mechanisms driving stick-slip described in this work and those of Kajiya et al. differ, the underlying recognition that stick-slip motion dominates contact line velocity on swelling hydrogels is a shared conclusion.

V. Conclusions

Due to the potential utility of thin hydrogel layers for microfluidic applications, it is important to understand their complex interactions with fluid flows. In this work, thin layers of PNIPAM coating a microchannel inner surface were shown to have significant impacts on capillary pressure driven flow of water. The filling time for water in a capillary coated with PNIPAM was three orders of magnitude larger than without the coating, and the filling velocity was constant. Given this linear dependence of meniscus position on propagation time, a stick-slip mechanism for water transport in swelling hydrogel coated capillaries has been proposed. In this framework, the contact line pins at the interface where water encounters dry and stiff polymer. This is due to a locally increased advancing contact angle, combined with elastic deformation of

the polymer surface, which lead to formation of a ridge arresting the fluid motion. Upon hydration of the polymer layer via water diffusion, the polymer softens, resulting in deformation relaxation and a decrease in the advancing contact angle, thereby unpinning the contact line as it rapidly slips forward. Once the contact line re-encounters dry hydrogel, it pins again and the process repeats itself. While this stick-and-slip process has been demonstrated in other circumstances, this study is the first to investigate repeated stick/slip events in a confined geometry, while also including mass exchange with the polymer substrate. The experimental findings and scaling predictions have important bearing on the growing numbers of applications which seek to use swelling polymers as smart, stimuli responsive coatings in microfluidic applications.

While the scaling argument presented is consistent with observations, the hypothesized sequence of events depicted in Fig. 8 has not been directly observed on a time scale of relevant individual steps. Future experiments accomplishing this visualization would be useful and enlightening if imaging with much greater temporal and spatial resolution can be achieved. Experiments with hydrogels of different elasticity would similarly be of great utility.

Of importance to practical applications, the synthesis methods devised for this work avoid specialized equipment and allow for application of these procedures for systems beyond basic cylindrical capillaries. For instance, a logical extension of this work would be to synthesize PNIPAM coatings in channels with different cross-sectional geometries (e.g., triangular, rectangular, etc.) in order to assess the effects of these shapes on contact line dynamics. This is important for practical applications that rely on capillary pumping for fluid routing and transport in confined microfluidic environment. An additional opportunity for further exploration is the use of controlled displacement filling to vary meniscus velocity. Finally, it would be very

interesting to investigate the impact of localized heating, bringing into play the thermal-responsive nature of PNIPAM on the control of capillary-pump water motion in a confined microfluidic environment enhanced with hydrogel lining of the channel walls.

Acknowledgements

Financial support by AFOSR BIONIC Center (awards No. FA9550-09-1-0162 and FA9550-14-1-0269), AFOSR FA9550-14-1-0015 Award and Georgia Tech's Renewable Bioproducts Institute Fellowship (JES) are acknowledged and appreciated. Technical input from Dr. Andrey Voevodin (AFRL) has been instrumental in performing this research.

References

1. M. A. C. Stuart, W. T. Huck, J. Genzer, M. Müller, C. Ober, M. Stamm, G. B. Sukhorukov, I. Szleifer, V. V. Tsukruk and M. Urban, *Nat Mater*, 2010, **9**, 101-113.
2. Y. Tanaka, J. P. Gong and Y. Osada, *Progress in Polymer Science*, 2005, **30**, 1-9.
3. S. Cuenot, S. Radji, H. Alem, S. Demoustier-Champagne and A. M. Jonas, *Small*, 2012, **8**, 2978-2985..
4. S. Rahimi, E. H. Sarraf, G. K. Wong and K. Takahata, *Biomedical microdevices*, 2011, **13**, 267-277.
5. S. Purushotham and R. V. Ramanujan, *Acta biomaterialia*, 2010, **6**, 502-510.
6. D. Subhash, H. Mody, R. Banerjee, D. Bahadur and R. Srivastava, 2011 11th IEEE Conference on Nanotechnology (IEEE-NANO), 2011, 1741-1744.
7. D. Kim and D. J. Beebe, *Lab on a chip*, 2007, **7**, 193-198.
8. A. Richter, S. Howitz, D. Kuckling and K.-F. Arndt, *Sensors and Actuators B: Chemical*, 2004, **99**, 451-458.
9. S. Ghosh, C. Yang, T. Cai, Z. Hu and A. Neogi, *Journal of Physics D: Applied Physics*, 2009, **42**.
10. F. Puoci, F. Iemma, U. G. Spizzirri, G. Cirillo, M. Curcio and N. Picci, *Am. J. Agric. Biol. Sci.* 2008, **3**, 299-314.
11. D. Schmaljohann, *Advanced Drug Delivery Reviews,* 2006, **58**, 1655-1670.
12. S. Dai, P. Ravi and K. C. Tam, *Soft Matter*, 2008, **4**, 435-449.
13. M. Zrínyi, *Colloid Polym Sci*, 2000, **278**, 98-103.
14. Y. Zhang and A. L. Yarin, *Journal of Materials Chemistry*, 2009, **19**, 4732-4739.
15. B. Ziolkowski, M. Czugala and D. Diamond, *Journal of Intelligent Material Systems and Structures*, 2013, **24**, 2221-2238.
16. T. Sun, G. Wang, L. Feng, B. Liu, Y. Ma, L. Jiang and D. Zhu, *Angewandte Chemie International Edition*, 2004, **43**, 357-360.
17. H. Ko, Z. Zhang, Y.-L. Chueh, E. Saiz and A. Javey, *Angewandte Chemie*, 2010, **122**, 626-629.
18. T. Young, *Philosiphical Transactions of the Royal Society of London,* 1804, **95**, 65-87
19. R. N. Wenzel, *Industrial & Engineering Chemistry*, 1936, **28**, 988-994.
20. A. B. D. Cassie and S. Baxter, *Trans. Faraday Soc.,*1944, **40,** 546-551.
21. J. Emile, A. Sane, H. Tabuteau and O. Emile, *Soft Matter*, 2013, **9**, 10229-10232.
22. B. B. J. Stapelbroek, H. P. Jansen, E. S. Kooij, J. H. Snoeijer and A. Eddi, *Soft Matter*, 2014, **10**, 2641-2648.
23. T. Kajiya, A. Daerr, T. Narita, L. Royon, F. Lequeux and L. Limat, *Soft Matter*, 2012, **9**, 454.
24. G. Pu and S. J. Severtson, *Langmuir*, 2008, **24**, 4685-4692.
25. G. Pu, J. Ai and S. J. Severtson, *Langmuir*, 2010, **26**, 12696-12702.
26. T. Kajiya, A. Daerr, L. Royon, L. Limat, T. Narita and F. Lequeux, *Soft Matter*, 2011, **7**, 11425-11432.
27. M. Stange, M. E. Dreyer and H. J. Rath, *Physics of Fluids*, 2003, **15**, 2587-2601.
28. B. Gorzolnik, P. Mela and M. Moeller, *Nanotechnology*, 2006, **17**, 5027-5032.
29. J. Zhang, R. Pelton and Y. Deng, *Langmuir*, 1995, **11**, 2301-2302.
30. R. W. Style, R. Boltyanskiy, Y. Che, J. Wettlaufer, L. A. Wilen and E. R. Dufresne, *Physical review letters*, 2013, **110**, 066103.
31. J. B. Bostwick, M. Shearer and K. E. Daniels, *Soft Matter*, 2014, **10**, 7361-7369.

32. S. Schmidt, M. Zeiser, T. Hellweg, C. Duschl, A. Fery and H. Möhwald, *Advanced Functional Materials*, 2010, **20**, 3235-3243.
33. S. Ohya, S. Kidoaki and T. Matsuda, *Biomaterials*, 2005, **26**, 3105-3111.
34. O. Tagit, N. Tomczak and G. J. Vancso, *Small*, 2008, **4**, 119-126.
35. K. Takahashi, T. Takigawa and T. Masuda, *The Journal of Chemical Physics*, 2004, **120**, 2972-2979.

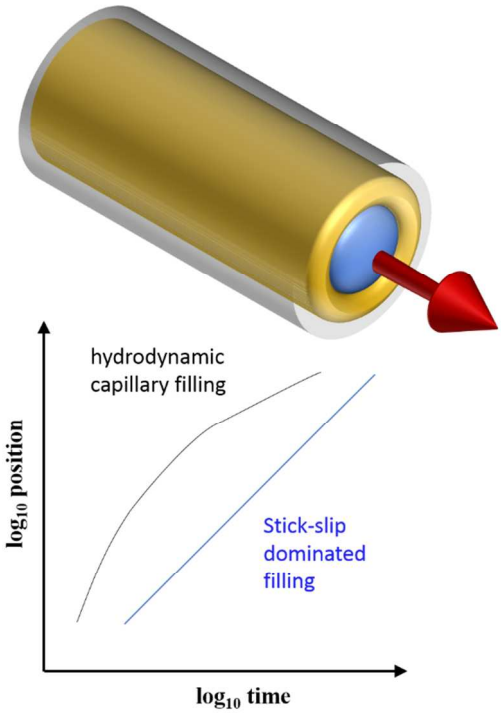

Capillaries coated with hydrogel on their inner wall fill via a stick-slip dominated process, with elastocapillary pining halting water meniscus motion, and polymer softening and increasing surface wettability initiating slip events.